Multiphysics simulation of thermoplastic polymer crystallization

Dear Author,

Please, note that changes made to the HTML content will be added to the article before publication, but are not reflected in this PDF.

Note also that this file should not be used for submitting corrections.

Materials and Design xxx (2015) xxx–xxx

Contents lists available at ScienceDirect

Materials and Design

journal homepage: www.elsevier.com/locate/matdes

Multiphysics simulation of thermoplastic polymer crystallization

Roberto Spina [a,b,*], Marcel Spekowius [b], Christian Hopmann [b]

[a] Dept. of Mechanics, Mathematics and Management (DMMM), Politecnico di Bari, Viale Japigia 182, 70126 Bari, Italy
[b] Institute of Plastics Processing (IKV), RWTH Aachen University, Pontstraße 55, 52062 Aachen, Germany

ARTICLE INFO

Article history:
Received 2 July 2015
Received in revised form 22 January 2016
Accepted 26 January 2016
Available online xxxx

Keywords:
Injection molding
Polymer
Crystallization
Numerical Simulation

ABSTRACT

The main goal of the presented work is to implement a robust framework for the computation of the crystallization kinetics of semi-crystalline thermoplastics by using a multiscale approach. The purpose of multiscale modeling is to assess parameters influencing microstructure formation that would otherwise require very time-consuming analysis with experiments. The numerical method, crystallization kinetics and their implementation into numerical software operating at macro- and micro-scale are described as well as the experimental data needed to prepare and validate numerical results.

1. Introduction

The manufacturing of high quality injection molded parts requires a deep understanding of material properties, process parameters and product design. The behavior of a polymer during the injection molding process and the performance of the final part are strongly determined by the material structure formed during filling and cooling. During processing, a polymer is normally subject to a complex thermo-mechanical history that leads to different microstructures at different locations, because of variations in shear rate, pressure and temperature. The prediction of the final microstructure is very important to attain manufacturing processes in which defects such as uncontrolled warpage, incorrect part dimensions, excessive weight, etc. are absent.

The complexity rises if semi-crystalline thermoplastics are used. These polymers tend to solidify in an ordered manner arranged in crystalline superstructures. Because of the length of the macromolecules, the material does not fully crystallize and amorphous domains coexist with crystalline ones. The manufacturing process influences the distribution of crystalline and amorphous areas as well as the crystalline superstructures. During solidification, the molecular chains, which are subject to high shear rates, have a much lower entropy than molecules which are unaffected by the flow. The decrease of entropy increases the free energy, which in turn implies an increase of the nucleation rate. In highly oriented melts, the solidification can result in a shish-kebab arrangement of the crystal lamellae. On the contrary, molecular chains located in quiescent regions form a spherulitic microstructure. Thus, the crystallization depends directly on melt flow and heat fluxes. Another influencing factor is inhomogeneities of the polymer melt such as variations in concentration, temperature and filling materials. Conversely, local variations of the crystallization rates influence melt properties, such as the viscosity. The polymer morphologies are also influenced from nucleating agents added with the aim to reduce dimensions of spherulites and improve mechanical properties (Lv et al. [1], Xu et al. [2]), the addition of another polymer to form a blend (An et al. [3]) or the mixing of the virgin material with recycled one (Madi [4]). The simulation of the crystallization process in injection molding is complex because it is necessary to combine transport phenomena of the multi-phase flow in non-isothermal conditions with crystallization kinetics. This requires the calculation of polymer properties on a microscopic scale using information from a macroscopic scale. It is possible to define this problem as a multiscale materials design problem. This means that the material is simulated from a micro-scale up to a macro-scale (Zeng et al. [5]). On each scale, particular material features have to be computed (Meijer and Govaert [6]). The crystallization problem can be considered as multi-scale problem in time and space. A spatial multi-scale problem involves more than one spatial scale to solve the associated sub-problems whereas a temporal multi-scale problem has different characteristic time scales. The coarse scale is needed to attain a feasible solution of the flow dynamic and melt behavior in a reasonable time while the fine scale is needed to improve knowledge on the local microstructures.

The main goal of the presented work is to implement a robust framework for the computation of the crystallization kinetics of semi-crystalline thermoplastics by using a multiscale approach. The purpose of multiscale modeling is to assess parameters influencing microstructure formation that would otherwise require very time-consuming

* Corresponding author at: Dept. of Mechanics, Mathematics and Management (DMMM), Politecnico di Bari, Viale Japigia 182, 70126 Bari, Italy.
E-mail address: roberto.spina@poliba.it (R. Spina).

http://dx.doi.org/10.1016/j.matdes.2016.01.123
0264-1275/

analysis thought experiments. The numerical method, crystallization kinetics and their implementation into numerical software operating at macro and micro scale are described as well as the experimental data.

2. Research background

The research on crystallization is actually focused on flow-induced crystallization. There are multiple models to compute interactions between fluid dynamics and crystallization, using approaches ranging from the simple modification of the quiescent crystallization coefficients to the use of micro-mechanical models. Dai et al. [7] investigated the influence of strain and strain rate on flow-induced crystallization for isotactic polypropylene. Experiments were carried-out on a rheometer operating in oscillatory mode. The results were compared with those achieved in continuous shearing with a thermal table mounted on an optical microscopy. The comparison illustrates that the rheological structures strictly depend on shear regime and rates. Koscher and Fulchiron [8] experimented on polypropylene to study the effect of shear on crystallization kinetics and morphology. The experimental protocol starts when the polymer is melted, afterwards a sufficient time applies for the homogenization. A fast cooling ramp is applied ten degree above the crystallization temperature, followed by a slow cooling ramp down to the crystallization temperature. Finally, the shear treatment is applied. Adopting this procedure, the quiescent crystallization model is extended to predict the shear treatment by linking the extra activated nuclei number to the first normal stress difference. The model is applied for the qualitative comparing of the behavior of polypropylene with different molecular weights. Ratajski and Janeschitz-Kriegl [9] studied the relation between nucleation densities and flow-induced crystallization. Increases in supercooling under quiescent conditions can significantly increase the number of nuclei. The supercooled state is of great importance for manufacturing processes on reducing the time needed for the full crystallization. The research shows that a specific amount of work is required to form Shish-Kebabs. Guo and Narh [10] proposed a simplified model of the flow-induced crystallization. The model, developed from the quiescent conditions, allows the experimental computation of a few parameter values to predict the flow-induced crystallization. The model computes the shift of the melt temperature towards higher values to take into account the shear effect. One of the main advantages of this model is the easy implementation into computational software to predict both stress-induced and quiescent crystallization. Zhou et al. [11] proposed a model in which the energy of dissipation strongly influenced the non-isothermal crystallization kinetics. The polymer flow influences the variation of the crystallization rate directly, applying the model of quiescent crystallization. Kim et al. [12] developed a flow-induced crystallization model, based on a thermodynamic point of view and a non-linear viscoelastic constitutive equation with a crystallization rate increased by flow. The thermodynamic model accounts for the increase of the melt temperature due to the entropy reduction for oriented melt. The non-linear viscoelastic constitutive equation is based on the Leonov model. This model allows the evaluation of the crystallinity with the variation of the processing parameters, computing the skin-layer thickness. However, the model cannot predict the effect of the fountain flow at the melt front. Zinet et al. [13] developed a numerical model to simulate the crystallization kinetics under non-isothermal conditions for the Couette shear flow configuration. The model takes into account that the flow-induced nucleation is directly influenced from the molecular orientation. The viscoelastic extra tensor quantifies the elastic part of the melt deformation and thus the molecular orientation. The model computes the evolution of the flow- and thermally-induced crystallization in function of the processing time separately. Another outcome of this model is the computation of the microstructures in the skin layer and core zone. The main limitation is the use of the spherulitic structures only. Zheng and Kennedy [14] and Zheng et al. [15] investigated the flow-induced crystallization during and after shearing. A finitely extensible nonlinear elastic dumbbell with Peterlin closure (FENE-P) is used to model polymer molecular orientation. The crystallizing system is considered as a suspension of semicrystalline structures growing and spreading from the amorphous matrix. The main result of the research is the identification of a new relation between the change in free energy due to flow and the nuclei generation of crystallization kinetics.

The multiscale analysis of the polymer crystallization is an important aspect to take into account. Shangguan et al. [16] proposed a two-scale model. One model describes the macro-flow, the second one is related to the short fiber movement. The macroscopic scale considers the basic macro-flow equations, including the continuity, motion and energy equations. The microscopic scale uses the dumbbell model equations to describe the evolution of micro-structural dynamics at molecular-level status. The microscopic information is reflected to the macroscopic one. This two scale model is applied to the analysis of fiber filled polymers. Rong et al. [17] presented a macro–micro model for the computation of the flow-induced crystallization in a simple shear flow. The macro analysis allows for the contribution of thermally induced nucleation, due to quiescent conditions, and the flow induced nucleation rate, due to flow conditions. The micro-analysis is used to describe a two-phase suspension model. The FENE dumbbell model and a rigid dumbbell model describe the amorphous phase and the semi-crystalline phase respectively. The multi-scale model is applied to simple Couette shear flow and it is limited to the spherulitical growth. Ruan et al. [18] investigated the cooling step of injection molding with a multiscale model. Two distinct length scales are used to simulate the crystallization: a coarse grid for the heat diffusion and a fine grid for capturing the crystal formation. The multi-scale model allows the 3D computation of temperature and relative crystallinity at various locations in the mold cavity as well as the evolution of the crystal morphologies. Wienke et al. [19] implemented a software to predict inner properties like the morphology of injection molded parts resulting from process parameters and geometry. The crystallization kinetics at micro level is coupled to existing injection molding software tools and structural analysis packages to perform computations at the macro level. The continuous data exchange between the two level allows the improvement of the numerical results. The model is able to investigate cooling in quiescent crystallization conditions. Complex geometries are repeated in small cells to allow the application of the model on computational heavy problem.

The review of the present literature points out that the research is focused on specific aspects of the polymer crystallization. Limited effort was spent to implement an integrated environment using multi-scale analysis to calculate the evolution of flow- and thermal-induced crystallization of the part during processing completely.

3. Problem modeling and numerical simulation scheme

The description of an incompressible (isochoric) viscous Navier–Stokes flow is based on the equations of conservation of mass, momentum and energy of a fluid occupying a dimensional region Ω:

$$\nabla \cdot \underline{u} = 0 \qquad \text{in } \Omega \tag{1}$$

$$\rho\left(\frac{\partial \underline{u}}{\partial t} + \underline{u} \cdot \nabla \underline{u}\right) = -\nabla p + \nabla \cdot \underline{\underline{\tau}} + \underline{f} \qquad \text{in } \Omega \tag{2}$$

$$\rho\left(\frac{\partial T}{\partial t} + \underline{u} \cdot \nabla T\right) = \nabla \cdot (k \nabla T) + \underline{\underline{\tau}} : \nabla \underline{u} + \rho \xi^{abs}_{max} \Delta H_c \frac{\partial \xi}{\partial t} \qquad \text{in } \Omega \tag{3}$$

where ρ is the density, $\underline{u}$ the velocity field, p the pressure, $\underline{\underline{\tau}}$ the viscous stress tensor, f the sum of the external forces, T the temperature, ΔH_c is

Please cite this article as: R. Spina, et al., Multiphysics simulation of thermoplastic polymer crystallization, Materials and Design (2015), http://dx.doi.org/10.1016/j.matdes.2016.01.123

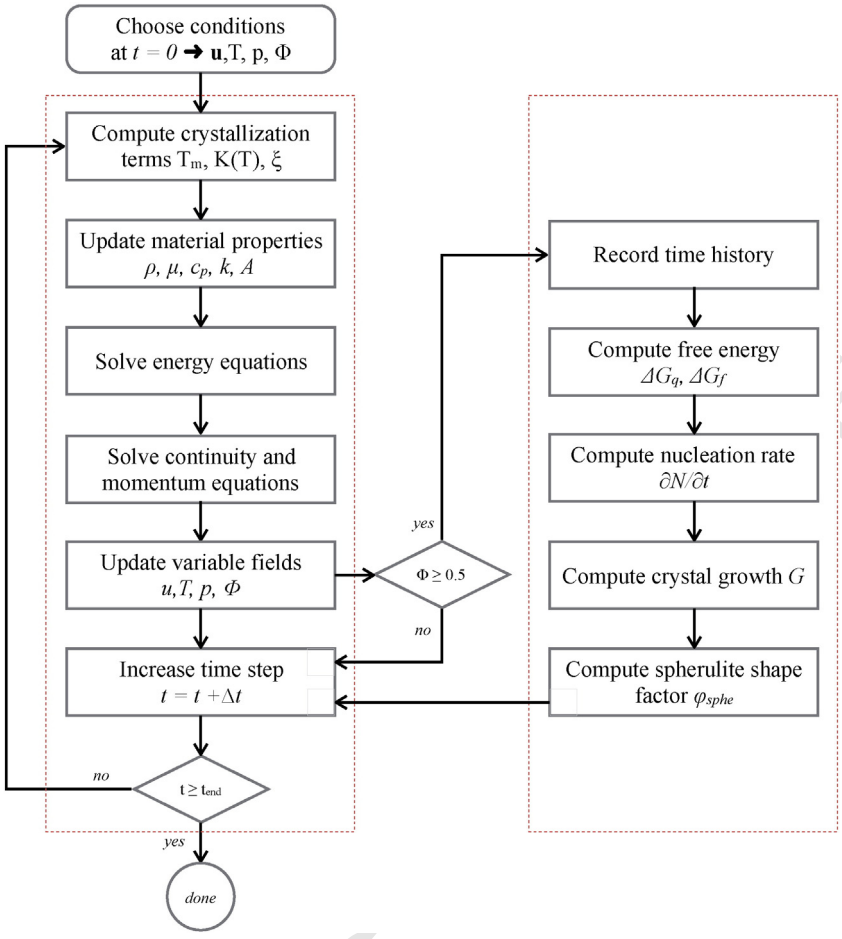

Fig. 1. Simulation flowchart.

the heat of crystallization, ξ the relative degree of crystallization and $\xi_{\max}^{abs}$ is the maximum value of the absolute degree of crystallization. The region Ω with the boundary $\Gamma = \partial\Omega$ denotes the geometrical domain where the spatial variables are valid. The pressure p appears only as a source term in the momentum equation, with no evolution equation associate to it. The pressure field is generally deduced in terms of the velocity field. The viscosity is related to the stress tensor by neglecting the conformation of the copolymers and viscoelastic effects.

$$\underline{\underline{\tau}} = \eta\underline{\underline{\gamma}} = \eta\left[\nabla\underline{u} + \nabla^T\underline{u}\right] \qquad \text{in } \Omega \tag{4}$$

where η is the viscosity.

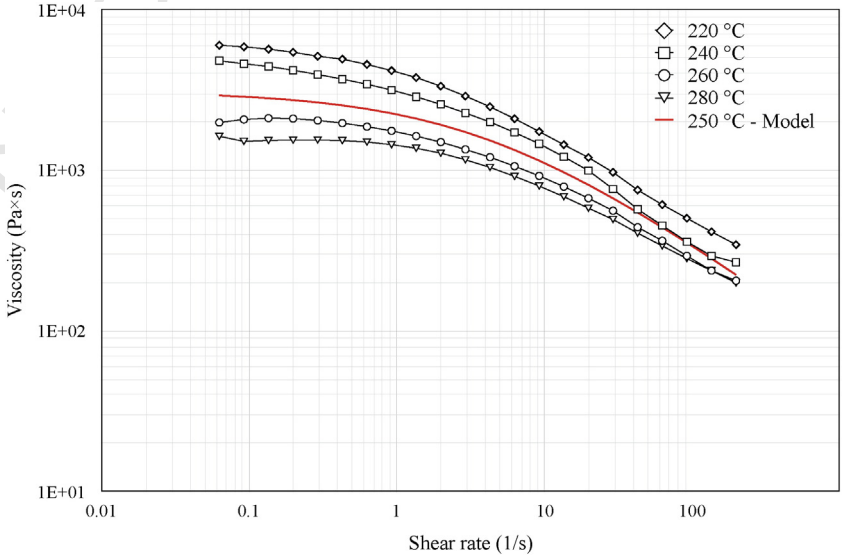

Fig. 2. Viscosity data.

Please cite this article as: R. Spina, et al., Multiphysics simulation of thermoplastic polymer crystallization, Materials and Design (2015), http://dx.doi.org/10.1016/j.matdes.2016.01.123

t1.1 **Table 1**
t1.2 Cross WLF coefficients.

t1.3 Parameter	Value
t1.4 τ^*	0.25 bar
t1.5 A_1	31.011
t1.6 A_2	51.6 K
t1.7 D_1	7.21×10^{10} bar × s
t1.8 D_2	1.1482 cm^3/g
t1.9 D_3	0 K/bar
t1.10 n	0.34

The system of equations also includes an equation of the multiphase flow that is needed to take into account the movement of the flow front repressing the interface between air and melt. The geometry consists of a union of multi domains Ω_i, one for each fluid. The moving interface, modeled as an iso-surface with a distance function representing the mutual distance between the two fluids, is computed with an evolved model of the level set method, originally introduced by Osher and Sethian [20]. In this work, the conservative equation of the level set method proposed by Olsson and Kreiss [21] and Olsson et al. [22] was used to avoid the problem of the mass loss during the flow front advancement. The level set function reads.

$$\frac{\partial \phi}{\partial t} + \underline{u} \cdot \nabla \phi = f(\phi) = \kappa \nabla \cdot \left[\varepsilon \nabla \phi - \phi(1-\phi) \frac{\nabla \phi}{|\nabla \phi|} \right] \qquad \text{on } \Gamma_{interface} = \Gamma_{polymer} \cap \Gamma_{air} \quad (5)$$

where ε is the parameter controlling the thickness of the transition region between the two fluids and κ is a stabilization term, necessary to maintain a hyperbolic tangent profile after the level set is transported. The level set function is usually initialized with a well know distance value to specify the initial interface and then periodically re-initialized imposing $|\nabla \phi| = 1$ during its evolution to achieve consistent ϕ values. In this way, a stable evolution is achieved and coherent results are ensured during the motion of this interface. For $\phi > 1/2$, the region is filled with polymer melt, for $\phi < 1/2$ it is filled with air while $\phi = 1/2$ locates the interface between the two fluids. The interfacial normal and curvature can be easily obtained by differentiating ϕ.

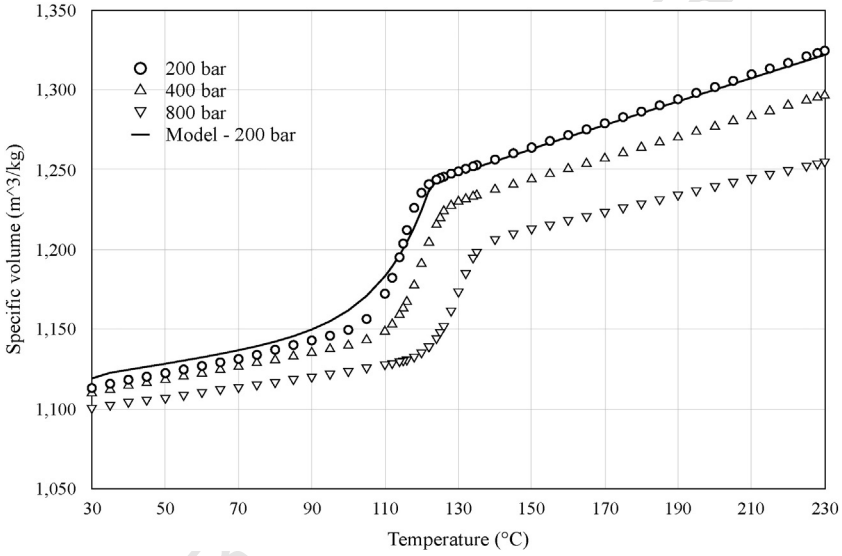

Fig. 3. pvT data with $\dot{T}_0 = 5$ °C/min.

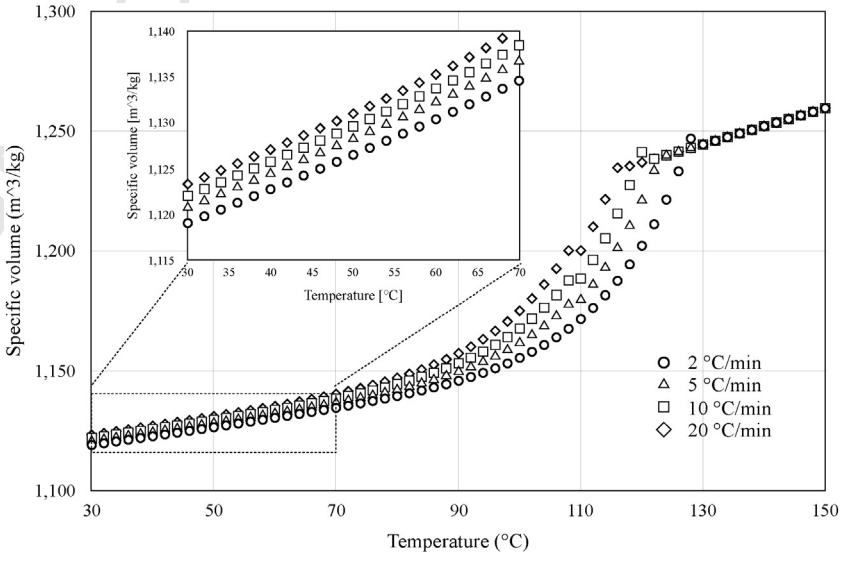

Fig. 4. pvT data with $p = 200$ bar.

Please cite this article as: R. Spina, et al., Multiphysics simulation of thermoplastic polymer crystallization, Materials and Design (2015), http://dx.doi.org/10.1016/j.matdes.2016.01.123

Table 2
pvT Tait data-fitted coefficients.

Parameter	Value
$b_{1,m}$	1.2586 cm^3/g
$b_{2,m}$	8.19×10^{-4} $cm^3/g/K$
$b_{3,m}$	904.31 bar
$b_{4,m}$	3.85×10^{-3} 1/K
$b_{1,s}$	1.1482 cm^3/g
$b_{2,s}$	2.73×10^{-4} $cm^3/g/K$
$b_{3,s}$	2.3513×10^3 bar
$b_{4,s}$	1.99×10^{-3} 1/K
b_5	392.71 K
b_5'	278.18 K
b_6	0.023 K/bar
b_7	0.1064 cm^3/g
b_8	0.076 1/K
b_9	2.12×10^{-3} 1/bar

Table 3
Thermal properties.

Parameter	Value
c_p at 60 °C	2.108×10^3 J/g/°C
c_p at 162 °C	3.187×10^3 J/g/°C
c_p at 175 °C	2.667×10^3 J/g/°C
c_p at 185 °C	2.698×10^3 J/g/°C
Δc_p at 162 °C	5.314×10^3 J/g/°C
α	2.5×10^3 $W/m^2/K$
λ at 60 °C	0.22 W/m/K

The crystallization process at macro-scale level is modeled using the Kolmogorov-Avrami-Evans (6) and Nakamura crystallization rate (7) equations

$$\xi = 1 - exp(-K(T) \cdot t^n) \tag{6}$$

$$\frac{d\xi}{dt} = n[K(T)]^{1/n}(1-\xi)[-\ln(1-\xi)]^{(n-1)/n} \tag{7}$$

where the degree of crystallization ξ is a function of the overall non-isothermal kinetic rate constant $K(T)$ and Avrami exponent n. The kinetic rate constant is implemented as a function only depending on the temperature which follows the Hoffman-Lauritzen (8) model with the correction proposed by Guo and Narh [10], as reported in Spina et al. [23]

$$K(T) = (\ln 2)^{1/n} \cdot \left(\frac{1}{t_{1/2}}\right) \cdot \exp\left(-\frac{U^*/R}{T - T_\infty}\right) \cdot \exp\left(-\frac{K_g}{T \cdot (T_m - T)} \cdot \frac{(T_m + T)}{2T}\right) \tag{8}$$

where U^* is the activation energy for the segmental jump rate in polymers, R is the ideal gas constant, K_g is the parameter associated to the spherulite growth rate, T_m and T_∞ are the equilibrium melt temperature and the temperature below which the diffusion stops. The crystallization process at micro-scale level is computed by calculating the nucleation rate dN/dt using the Lauritzen and Hoffman [24] approach

$$\dot{N} = C \cdot k_B \cdot T \cdot \Delta G \cdot \exp\left(-\frac{E_a}{k_B \cdot T}\right) \cdot \exp\left(-\frac{K_n}{T \cdot (\Delta G)^n}\right) \tag{9}$$

with C and K_n as material constants, k_B the Boltzmann constant, ΔG the free Energy and E_a an activation energy of the supercooled liquid-nucleus interface. The exponent n can assume the values 1 or 2 depending on the temperature region in which the homogenous nucleation takes place. The crystal growth process is simulated by using the Hoffman, Davis and Lauritzen [25] model

$$G = G_0 \cdot \exp\left(-\frac{U^*/R}{T - T_\infty}\right) \cdot \exp\left(-\frac{K_g}{T \cdot \left(T_m^0 - T\right)} \cdot \frac{(T_m + T)}{2T}\right) \tag{10}$$

with G_0 as a material constant and T_m^0 the equilibrium melt temperature in quiescent condition. It should be pointed out that the growth speed G of the crystal growth front is assumed independent of the flow field. Thus, it only depends on the temperature field and the material parameters.

The crystallization of polymeric materials is a solidification process in strong interaction with heat conduction. The nucleation and growth

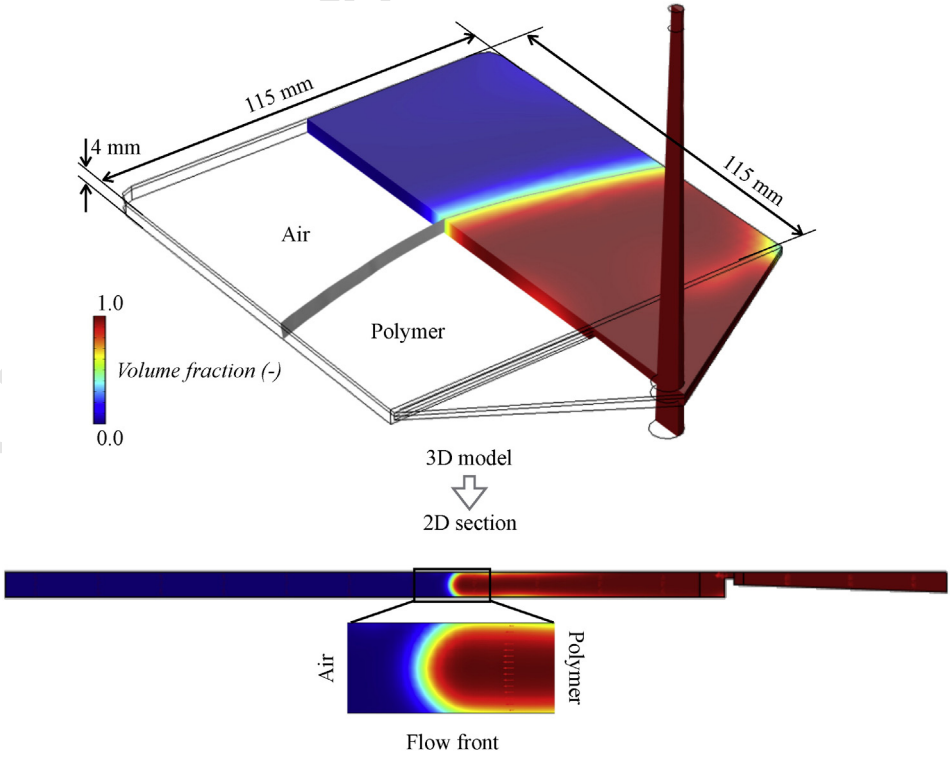

Fig. 5. Flow front advancement (2.1/220/40).

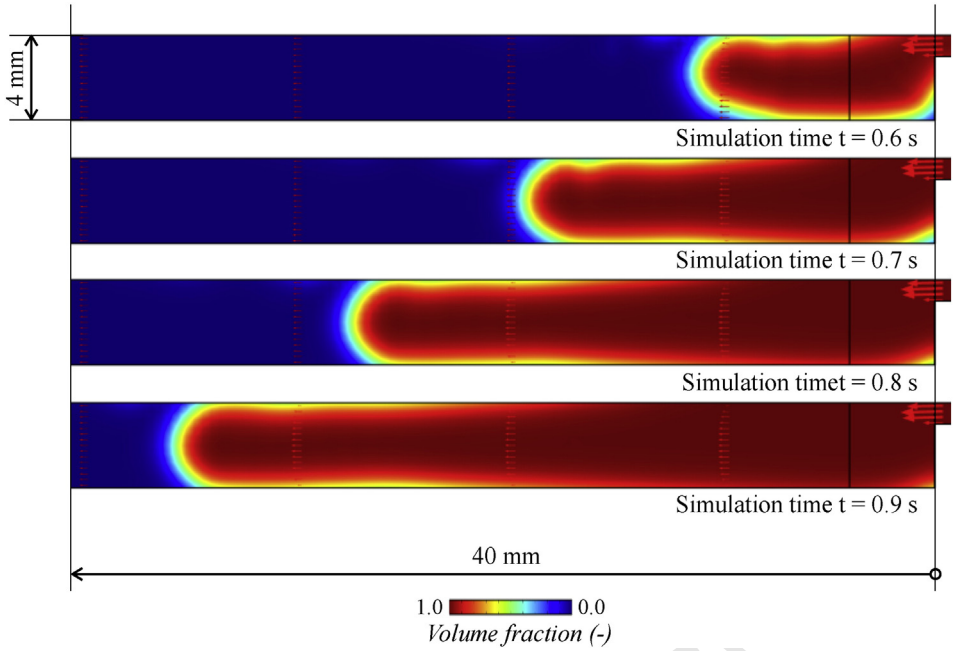

Fig. 6. Flow front evolution (2.1/220/40).

of spherulites are strongly influenced by the temperature and its variation. Vice versa, the material properties depend on the developed microstructure and it causes a considerable change in the flow and heat transfer processes. For this reason, the main material properties are computed as a function of the relative crystallization degree. Considering that polymers never crystallize completely, the rule of mixture is applied between the ideal polymer crystal (relative degree of crystallization ξ equal to 1) and the complete amorphous one (relative degree of crystallization ξ equal to 0), using the equation:

$$f = f_{crystal} \cdot \xi \cdot \xi_{max}^{abs} + f_{amorphous} \cdot (1 - \xi) \cdot \xi_{max}^{abs} \quad (11)$$

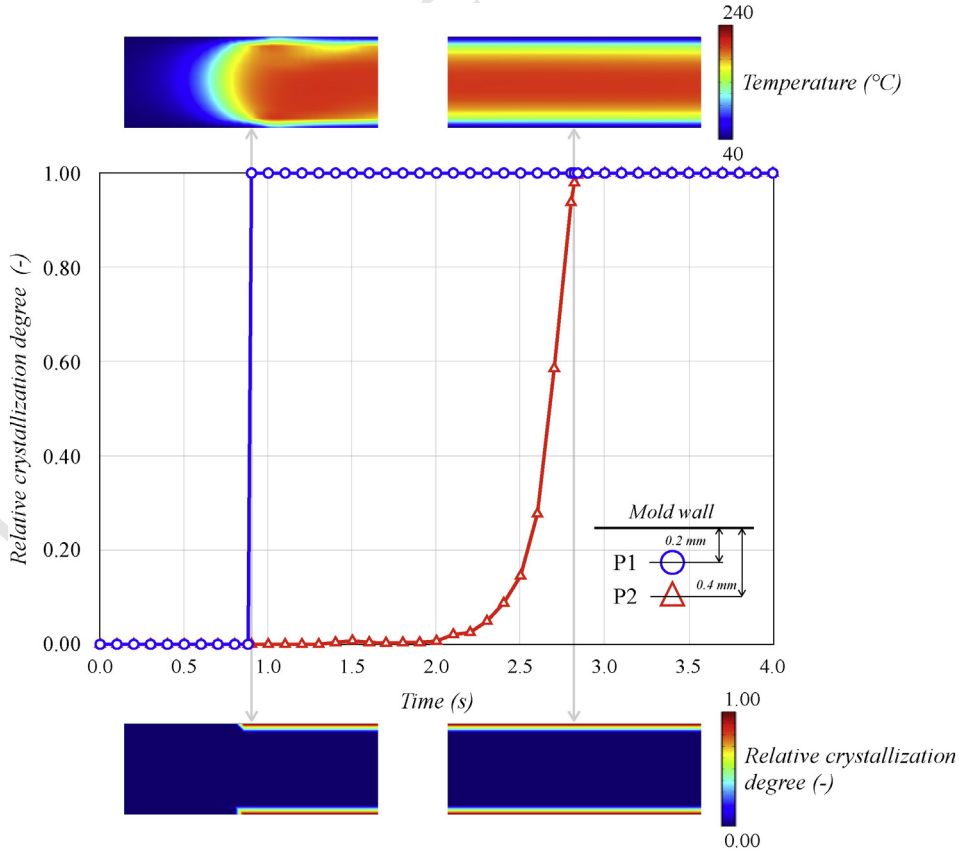

Fig. 7. Relative crystallization degree (2.1/220/40).

Please cite this article as: R. Spina, et al., Multiphysics simulation of thermoplastic polymer crystallization, Materials and Design (2015), http://dx.doi.org/10.1016/j.matdes.2016.01.123

Table 4
Statistical experimental plan.

Pattern	ID	Injection time (s)	Injection temperature (°C)	Mold temperature (°C)	Avg diameter Core (μm)	Avg diameter Skin (μm)
++−	2.1/280/40	2.1	280	40	39.93	31.70
−++	1.0/280/80	1.0	280	80	64.86	66.86
+−+	2.1/220/80	2.1	220	80	68.91	70.05
−−−	1.0/220/40	1.0	220	40	37.04	27.31
+−−	2.1/220/40	2.1	220	40	39.63	28.11
−+−	1.0/280/40	1.0	280	40	39.44	27.82
−−+	1.0/220/80	1.0	220	80	64.78	74.47
+++	2.1/280/80	2.1	280	80	61.28	71.16

where f is a general material property and $\xi_{\max}^{abs}$ the maximum absolute crystallization degree, measure with the differential scanning calorimetry (DSC) technique. $F_{amorphous}$ is only depending on the temperature while $f_{crystal}$ is a function of temperature and crystallization parameters. Applying the above rule of mixture, the material's specific heat and thermal conductivity read

$$c_p = c_{p,crystal} \cdot \xi \cdot \xi_{max}^{abs} + c_{p,amorphous} \cdot (1-\xi) \cdot \xi_{max}^{abs} \quad (12)$$

$$k = k_{crystal} \cdot \xi \cdot \xi_{max}^{abs} + k_{amorphous} \cdot (1-\xi) \cdot \xi_{max}^{abs} \quad (13)$$

A suspension-based rheological model is applied to compute the viscosity η as a function of the crystallization degree

$$\eta = \eta_{amorphous} \cdot \left(1 - \frac{\xi \cdot \xi_{max}^{abs}}{\varphi_{sphe}}\right)^{-B\varphi_{sphe}} \quad (14)$$

where B is the Einstein coefficient and φ_{sphe} is the spherulite volume fraction, in analogy to what was reported by Mueller et al. [26]. The viscosity of this suspension depends on fluid-dynamic and particle-particle interactions as well as particle shape and orientation. The amorphous viscosity is represented by a Cross-WLF viscosity model (William et al. [27]) as a function of the temperature, shear rate, and pressure.

$$\eta_{amorphous} = \eta_0 \cdot \left(1 + \left(\frac{\eta_0}{\tau^*} \cdot \dot{\gamma}\right)^{1-n_v}\right)^{-1} \quad (15)$$

with

$$\eta_0 = D_1 \cdot \exp\left(-A_1 \frac{T - D_2}{A_2 + T - D_2}\right) \quad (16)$$

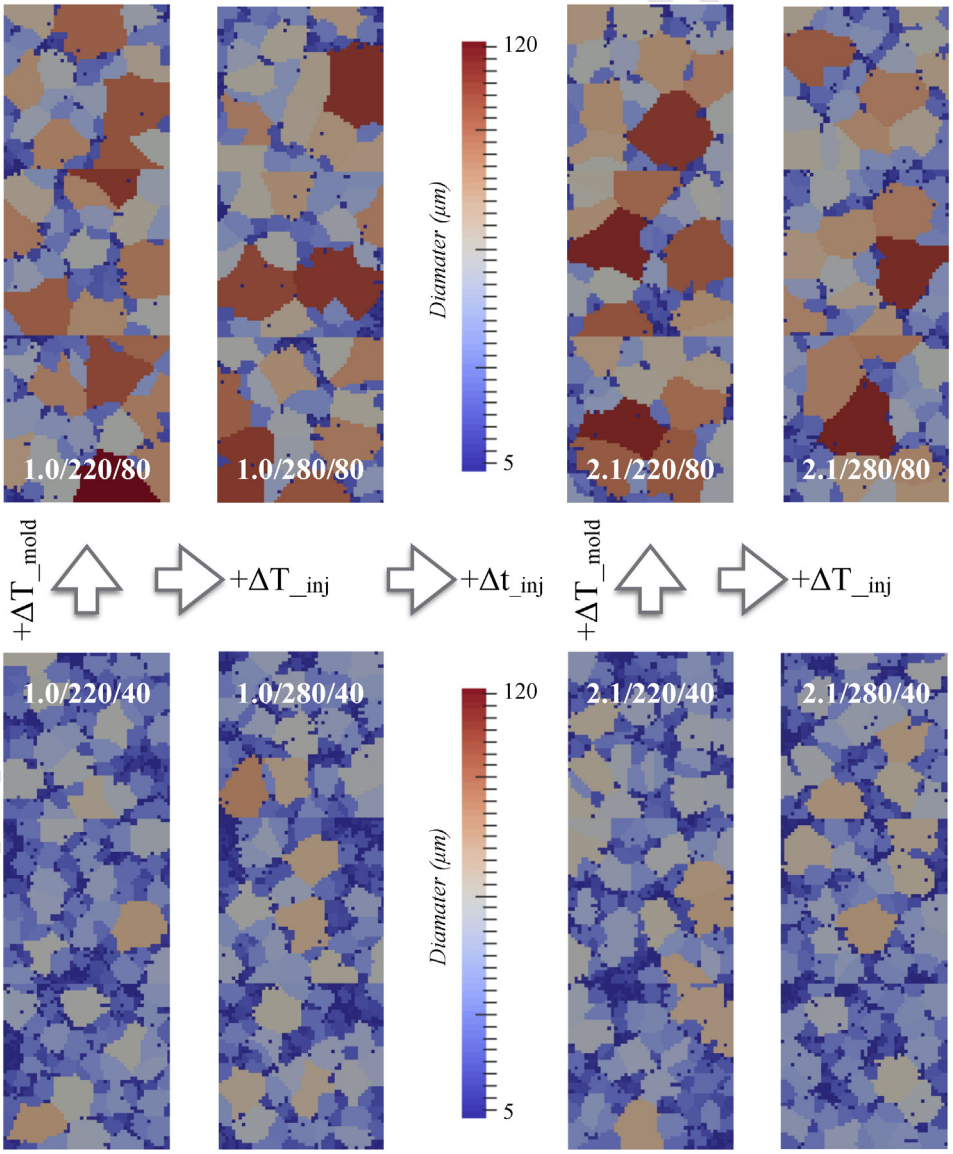

Fig. 8. Spherulite simulation - in the core.

Please cite this article as: R. Spina, et al., Multiphysics simulation of thermoplastic polymer crystallization, Materials and Design (2015), http://dx.doi.org/10.1016/j.matdes.2016.01.123

where η_0 is the zero shear viscosity in which the viscosity approaches a constant level at very low shear rates, τ^* the critical stress level at the transition to shear thinning, n_v the power law index in the high shear rate regime, A_1, A_2, D_1 are data-fitted coefficients and D_2 is the glass transition temperature.

The polymer specific volume, necessary to account for material compressibility during a flow simulation, equals

$$\rho^{-1} = v\left(T,p,\dot{T}\right) = v_0\left(T,\dot{T}\right)\cdot\left[1 - C\cdot\ln\left(1+\frac{p}{B\left(T,\dot{T}\right)}\right)\right] + v_t\left(T,p,\dot{T}\right) \tag{17}$$

with the variation of temperature T, pressure p and cooling rate $\dot{T}$ by using a modified dual-domain Tait equation, as reported in Spina et al. [28]. The introduction of the cooling rate factor in the equation is needed to predict material behavior for different cooling rate conditions and take into account the influence of crystallinity.

The unknowns in the thermo-fluid dynamic problem are the velocity, temperature and interface distance fields. The velocity boundary conditions are.

$$\underline{u}|_t = \underline{u}_{inlet} \qquad \text{on } \Gamma_{inlet} \tag{18}$$

$$\underline{u}\cdot\underline{n}|_t = f(\phi) \qquad \text{on } \Gamma - \Gamma_{inlet} - \Gamma_{outlet} \tag{19}$$

$$\underline{u}|_t = \underline{0} \qquad \text{on } \Gamma_{outlet} \tag{20}$$

where $\underline{u}_{inlet}$ is the velocity profile set at polymer entrance.

The temperature boundary conditions are.

$$T|_t = T_{inj} \qquad \text{on } \Gamma_{inlet} \tag{21}$$

$$T|_{t=0} = T_{mold} \qquad \text{on } \Gamma - \Gamma_{inlet} \tag{22}$$

$$-\underline{n}\cdot(k\nabla T) = h\cdot(T_{mold} - T) \qquad \text{on } \Gamma - \Gamma_{inlet} \tag{23}$$

where *inlet* and *outlet* denote the entry and exit position of fluids, and h is the transfer coefficient, as specified in Spina et al. [...].

The interface distance at the initial time is well-known and equals.

$$\frac{\partial\phi}{\partial t} + \underline{u}\cdot\nabla\phi\Big|_{t=0} = \frac{1}{2} \qquad \text{on } \Gamma_{interface} = \Gamma_{polymer}\cap\Gamma_{air} \tag{23}$$

Particular attention was paid on specifying the velocity at the mold wall for the two fluids. In particular, a non-slip condition was applied when the polymer was in contact with the mold while a free slip condition was applied for air. This particular boundary condition was implemented by using an adjustable Robin boundary condition as a function of the level set variable ϕ,

$$\underline{u} + \zeta(\phi)\frac{\partial\underline{u}}{\partial t} = \underline{0} \qquad \text{on } \Gamma_{wall} \tag{24}$$

where the function $\zeta(\phi)$ is a smooth transition between the values 0 and 10^5 at $\phi = ½$ to avoid convergence problem because of drastic change of the velocity condition.

The boundary conditions of the holding phase are the application of the pressure on the inlet.

$$p = p_{holding} \qquad \text{on } \Gamma_{inlet} \tag{25}$$

and a zero pressure gradient in the normal direction to the mold boundary.

$$\frac{\partial p}{\partial n} = 0 \qquad \text{on } \Gamma_{wall} \tag{26}$$

4. Numerical simulation

The numerical analyses were performed at both macro- and micro-scale in order to predict the injection molding process in a better way. The governing equations were discretized with a Finite Element Method and approximate solutions computed for the discrete nodal values of the melt and air domains. A flowchart illustrating the computed steps is shown in Fig. 1. This diagram depicts the process by which a

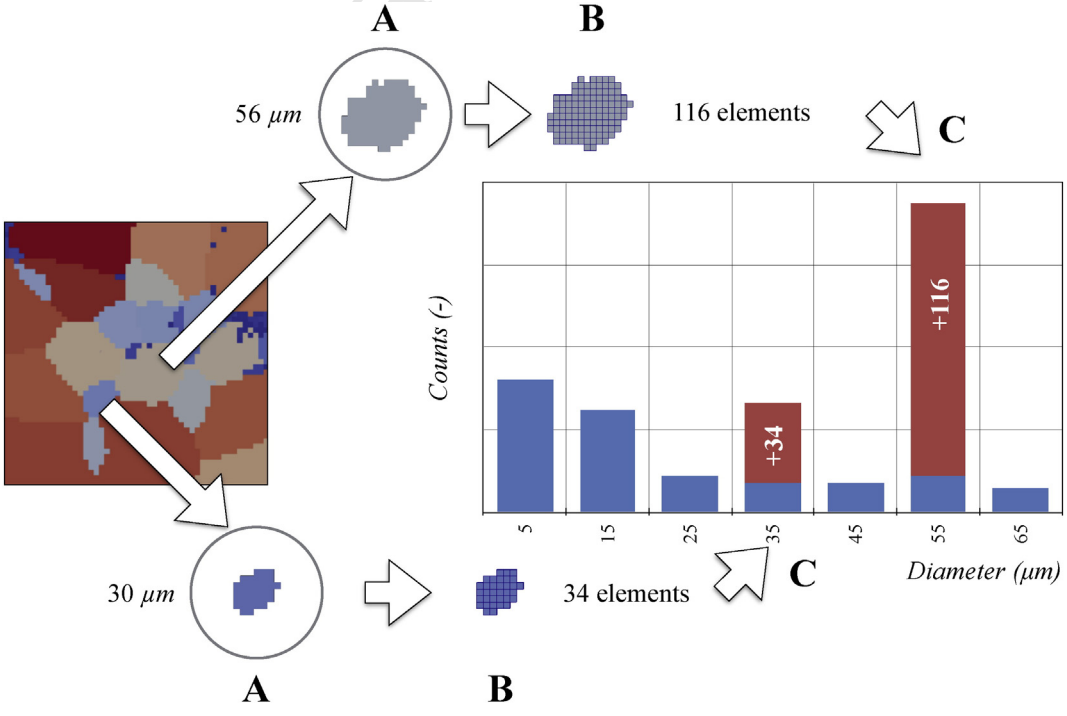

Fig. 9. Areal computation.

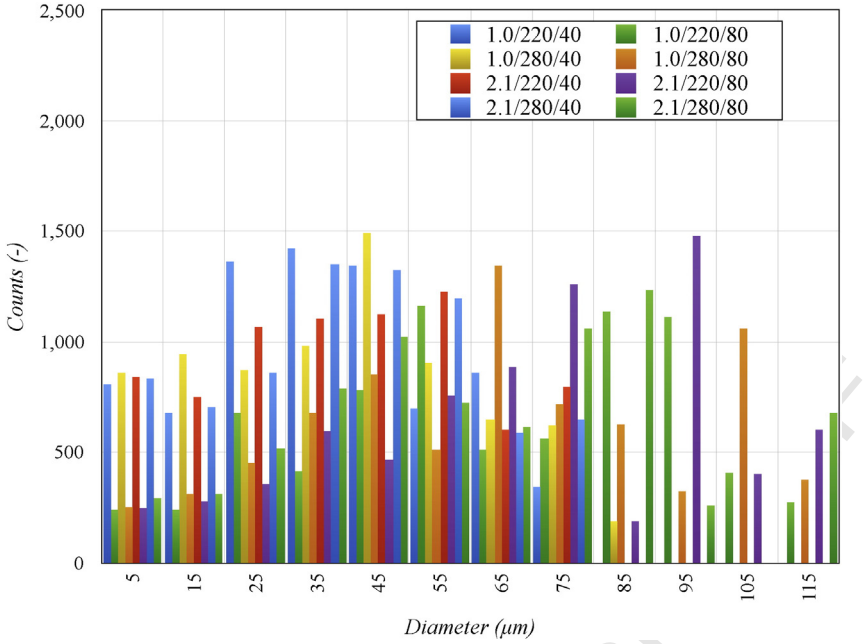

Fig. 10. Spherulite size distributions - in the core - areal distribution.

segregated algorithm solves the energy, continuity and momentum equations, for the unknown variables fields at a given time. When the multi-phase flow equations are coupled together, the coefficients are computed for each equation.

At the initial time step $t = 0$, the boundary conditions are imposed and the velocity u, temperature T, pressure p and level set variable ϕ are initialized. The main crystallization terms were evaluated and the material properties updated. In this initial stage, the material properties are those of the polymer melt. The equation of energy is initially computed and then the continuity and mass equations by using a segregated solver in which the complete Jacobian matrix was split into smaller sub-problems. In the first sub-problem, the temperature field was calculated whereas the second sub-problem solves the velocity, pressure and level set variable. In this way, the computational effort and solution time were reduced. The tradeoff with respect to computational resources was that the segregated solver required less memory per cell than the fully coupled solver. If the level set variable was less than 0.5, the simulation time was increased and the computation cycle repeated. On the contrary, the micro-scale solver SphäroSim was used for the calculation. The initial step of the simulation was to record the time history because the stress in a fluid element depends on the entire deformation history. The crystallization was simulated using a cellular automaton for which the original hexaeder mesh was subdivided into a high-resolution mesh. Each element of the high-resolution mesh represented the phase state of a small volume in the simulation area. The phase state was 'solid' if the element was part of a crystalline superstructure, otherwise it was 'melt'. A nucleation rate was calculated by applying Eq. (9) and used to compute a time-dependent nuclei distribution. The Gibbs free energy is split in a quiescent part ΔG_q and a flow induced part ΔG_f, which can be calculated from the given temperature and velocity fields. ΔG_q is derived from steady-state conditions whereas the reptation theory is applied for the flow induced part ΔG_f. The crystal growth process is simulated by using Eq. (10). The shape factor is then computed. A detailed description of the algorithms used to calculate the crystallization process on a micro-scale is given in Spekowius et al. [29].

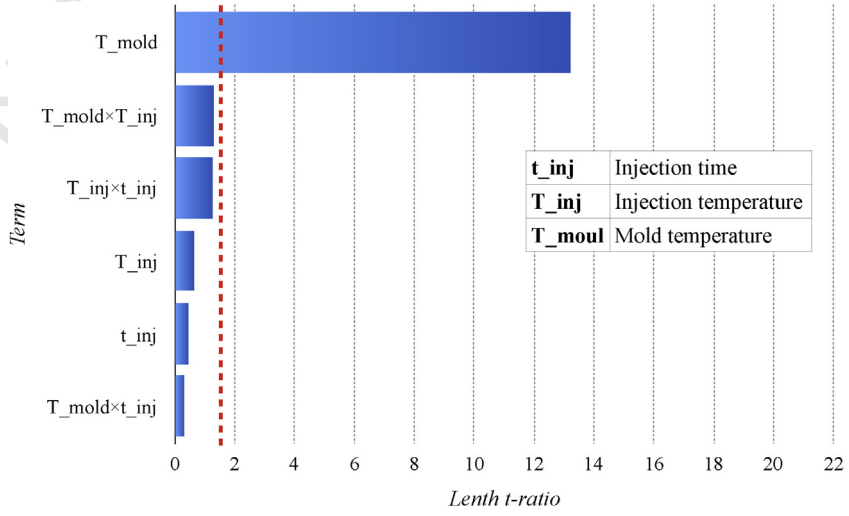

Fig. 11. Pareto chart — in the core.

Please cite this article as: R. Spina, et al., Multiphysics simulation of thermoplastic polymer crystallization, Materials and Design (2015), http://dx.doi.org/10.1016/j.matdes.2016.01.123

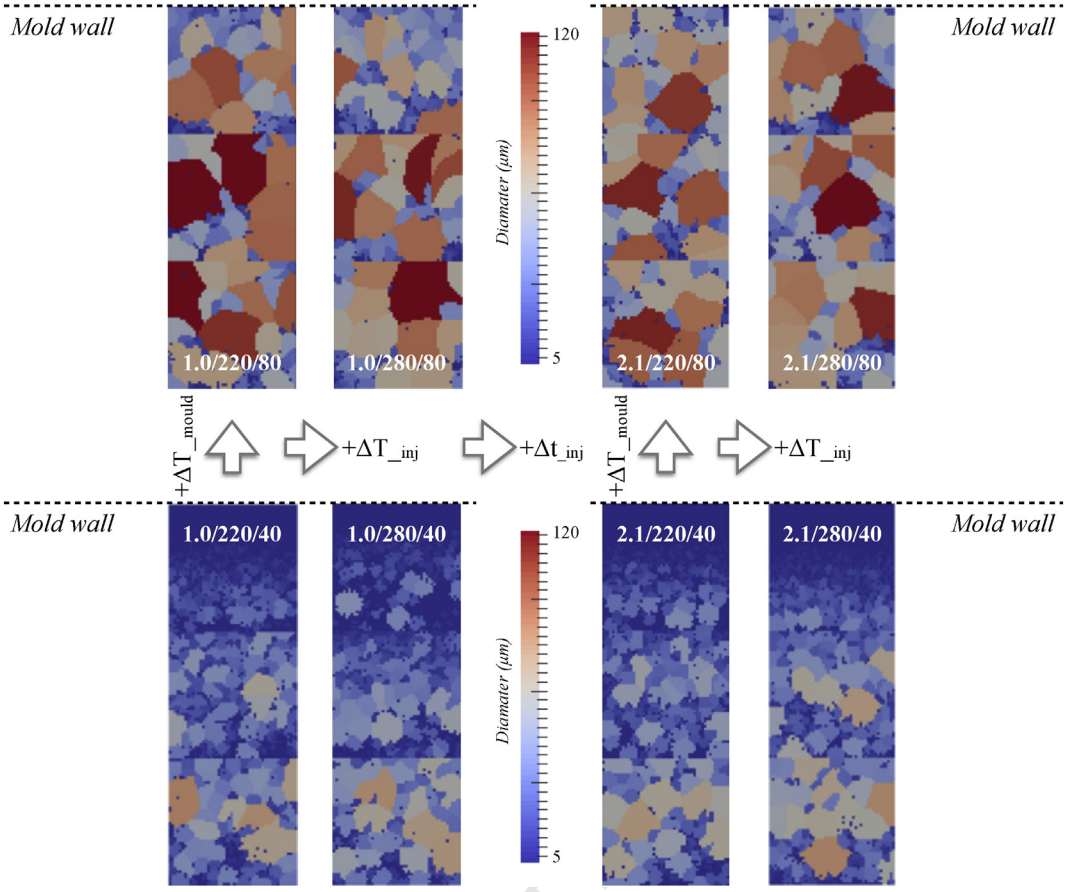

Fig. 12. Spherulite simulation — at skin.

5. Material characterization

An isotactic polypropylene was chosen as semi-crystalline thermoplastic polymer. The material was the PP 505 P produced by SABIC AG (Bergen op Zoom, Netherlands) with a specific density of 0.905 g/cm^3 and melt flow index of 2.0 g/10 min. This material is characterized by a glass transition temperature of $T_g = -10$ °C and an equilibrium melt temperature of $T_m^0 = 200$ °C. The activities of the material characterization contained the viscosity, pressure-specific volume-Temperature data and crystallization data.

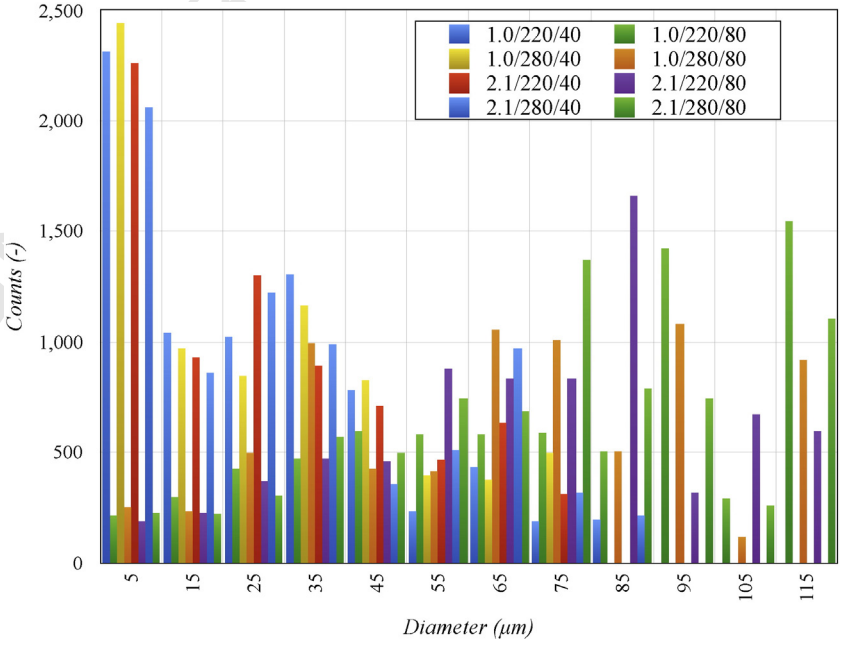

Fig. 13. Spherulite size distributions — at skin — areal distribution.

Please cite this article as: R. Spina, et al., Multiphysics simulation of thermoplastic polymer crystallization, Materials and Design (2015), http://dx.doi.org/10.1016/j.matdes.2016.01.123

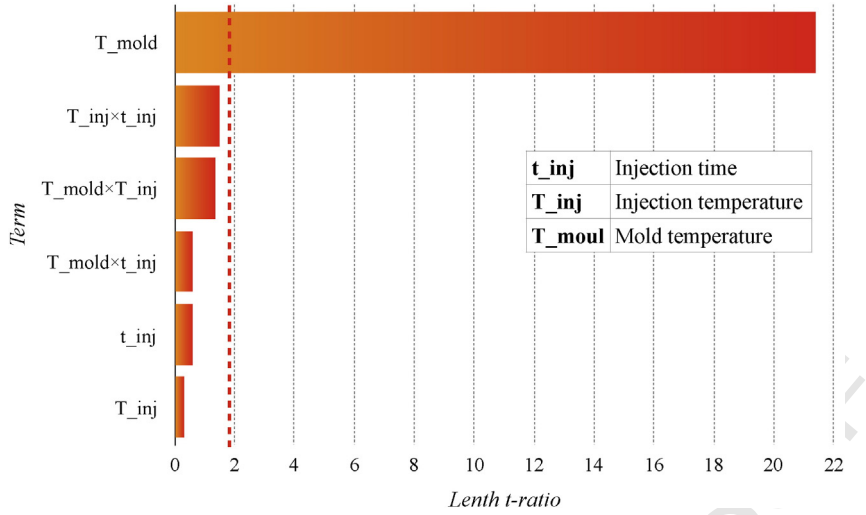

Fig. 14. Pareto chart — at skin.

The viscosity was measured in the range between 220 and 280 °C by using an HAAKE MARS III rotational rheometer of Thermo Fisher Scientific Inc. (Waltham, MA, USA) in a plate-plate configuration (diameter equal to 25 mm) under nitrogen atmosphere. The experiment protocol was divided into two steps. In the first step, amplitude sweep tests were performed to identify a stable linear viscoelastic region of the material, whereas in the second step frequency sweep tests were carried-out to measure the polymer viscosity. A stable common linear region was identified for shear values between 10^{-3} and 10^{-2}. For this reason, the following frequency sweep tests were carried out with a shear value equal to 5×10^{-3}. A frequency sweep is a particular test useful to determine the viscoelastic properties of a material as a function of timescale. Cox and Merz [30] established a strict equivalence between the complex viscosity $\eta^*(\Omega)$ measured in an oscillatory frequency sweep (at a fixed strain amplitude within the linear viscoelastic regime) and the steady shear viscosity $\eta(\dot{\gamma})$ measured as a function of shear rate $\dot{\gamma}$. Applying this equivalence, the polymer viscosity is obtained. Fig. 2 reports the viscosity measurements, carried out with shear rate ranging between 6×10^{-2} and 2×10^{2} s^{-1}. The curves with symbols are the experimental data whereas the curve without the symbol is the model-prediction at a specific temperature. The data fitted coefficients of the Cross WLF are reported in the Table 1.

The pressure-specific volume-Temperature (pvT) data provides information about the specific volume changes. It was measured using a pvT-100 device of SWO Polymertechnik GmbH (Krefeld, Germany) using testing pressures and cooling rates ranging between 10^2 and 10^3 bar and 1 and 40 °C/min respectively. Fig. 3 reports the pvT measurements and the model prediction for a cooling rate of 5 °C/min, used as reference value $\dot{T}_0$.

The effect of the cooling rate is strictly related to the degree of crystallinity. As the degree of crystallinity increases with a decrease of the cooling rate, the specific volume decreases because of the additional densification, which is due to the growing crystal structure in the polymer. In addition, the transition temperature is shifted to lower values with the increase of the cooling rate. Fig. 4 shows the specific volume as a function of temperature for values of the cooling rate of 2, 5, 10 and 20 °C/min and a constant pressure of 200 bar.

The graph detail points out the increase of the specific volume with the decrease of the cooling rate in the range of 30–70 °C, confirming the results of Zuidema et al. [31]. The data fitted coefficients of the modified dual-domain Tait equation are reported in the Table 2.

Additional material properties such as the thermal conductivity and specific heat are reported in Table 3. More details can be found in Spina et al. [28].

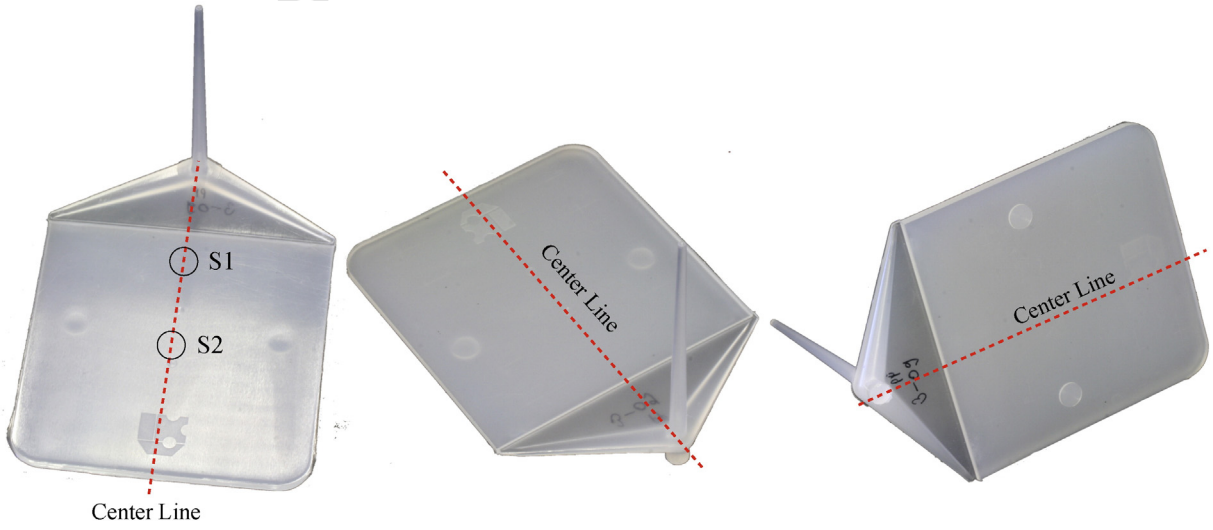

Fig. 15. Manufactured part.

Please cite this article as: R. Spina, et al., Multiphysics simulation of thermoplastic polymer crystallization, Materials and Design (2015), http://dx.doi.org/10.1016/j.matdes.2016.01.123

6. Analysis of results

The chosen part was a rectangular plate with a volume of $115 \times 115 \times 4\ mm^3$. The processing parameters considered as constants were the holding pressure (70% of the maximum injection pressure), the holding time (5 s) and the cooling time (55 s). The injection time ranged between 1.0 and 2.1 s, melt temperature between 220 and 280 °C, and mold temperature between 40 and 80 °C. To accurately compute the polymer/air interface and the slip/no slip condition at the mold wall, the mesh size used for the macro-scale simulation was equal to 100 μm. Each simulation run is identified by a triplet set (injection time *t_inj*/fill temperature *T_inj*/mold temperature *T_mold*). The melt-front advancement (Fig. 5) shows the evolution of polymer flow front as the part fills for the parameter set (2.1/220/40). The polymer melt entered into the part from the gate, far from the initial interface polymer-air positioned in the sprue. Since the part is characterized by a uniform cross-sectional area, a constant velocity was developed and stationary conditions could be achieved after a short time.

Observing the different images of the filling phase (Fig. 6), a smooth representation of the polymer fill region is achieved with the level set method. In addition, the air entrapments are located in the areas where the velocity components were very low. Results for a simulation time of 0.9 s beginning at the start of filling are shown in the figure. Q4

The volume fraction is a function of the level set variable and assumes a value equal to one when the polymer occupies the region and equals zero for the air. The temperature field, coupled to the volume fraction field, has a slight different shape for the heat fluxes between the polymer, air and mold material. The polymer in contact with the mold walls rapidly froze because of the high thermal gradient, creating a thin insulating layer and allowing the temperature in the core to

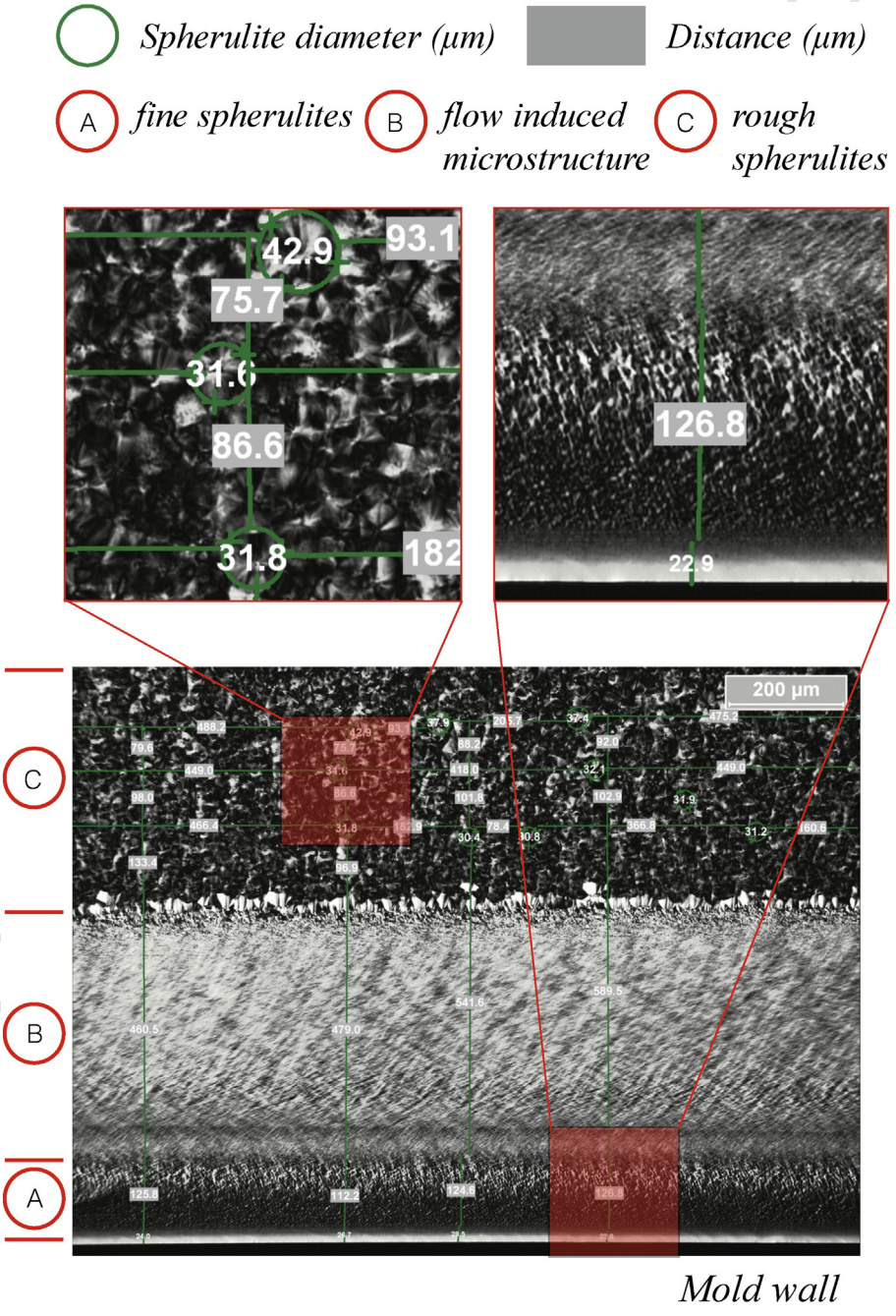

Fig. 16. Sections at *S1* location — lengthwise.

Please cite this article as: R. Spina, et al., Multiphysics simulation of thermoplastic polymer crystallization, Materials and Design (2015), http://dx.doi.org/10.1016/j.matdes.2016.01.123

remain constant. The air in contact with the flow front cooled down the polymer melt but the thermal gradient was too low to solidify the polymer melt. As a result, the absolute crystallization degree, as a function of volume fraction and temperature fields, is equal to the maximum value of 0.53 at the mold walls and 0.00 in the core. As Fig. 7 discloses, the analysis was extended to the entire simulation period. The points *P1* and *P2* were located along the thickness at 0.2 and 0.4 far from the mold surface. The crystallization degree of *P1* reached the maximum value 0.9 s after the start of filling. The transformation was instantaneous. On the contrary, the crystallization of *P2* was smooth, because the temperature decrease was less rapid. Based on these results, coarse microstructure (large spherulites) is expected at the core due to the slow cooling conditions, while fast cooling at the mold wall determines an amorphous phase with a very fine structure (small spherulites) at the mold walls.

However, the results do not provide any direct information on the spherulite dimensions and distribution. To compute the real microstructure, the micro-scale simulation was performed with the process parameters of the statistical experimental plan reported in Table 4.

The spherulites in the core were computed on a reference domain area of 200 × 600 μm^2 and subdivided into small square elements (length of 4 μm). The initial nuclei are located at the centers of each square element and the spherulites grow out from these positions during the crystallization process. Fig. 8 shows the simulated microstructures for different values of the process parameters. The results point out that an increase of the mold temperature causes an increase of the spherulite size whereas an increase of the injection time and/or melt temperature has a limited effect on the spherulite size.

The areal distribution was computed for each reference domain to evaluate the importance of each factor with the statistical analysis by following the procedure, which is shown in Fig. 9. The procedure starts with the spherulite selection and the computation of the diameter of its surrounding bounding sphere (step A). The number of elements with an area of 16 μm^2 are identified for the selected spherulite (step B) and then collected into the distribution graph (step C). All spherulite sizes

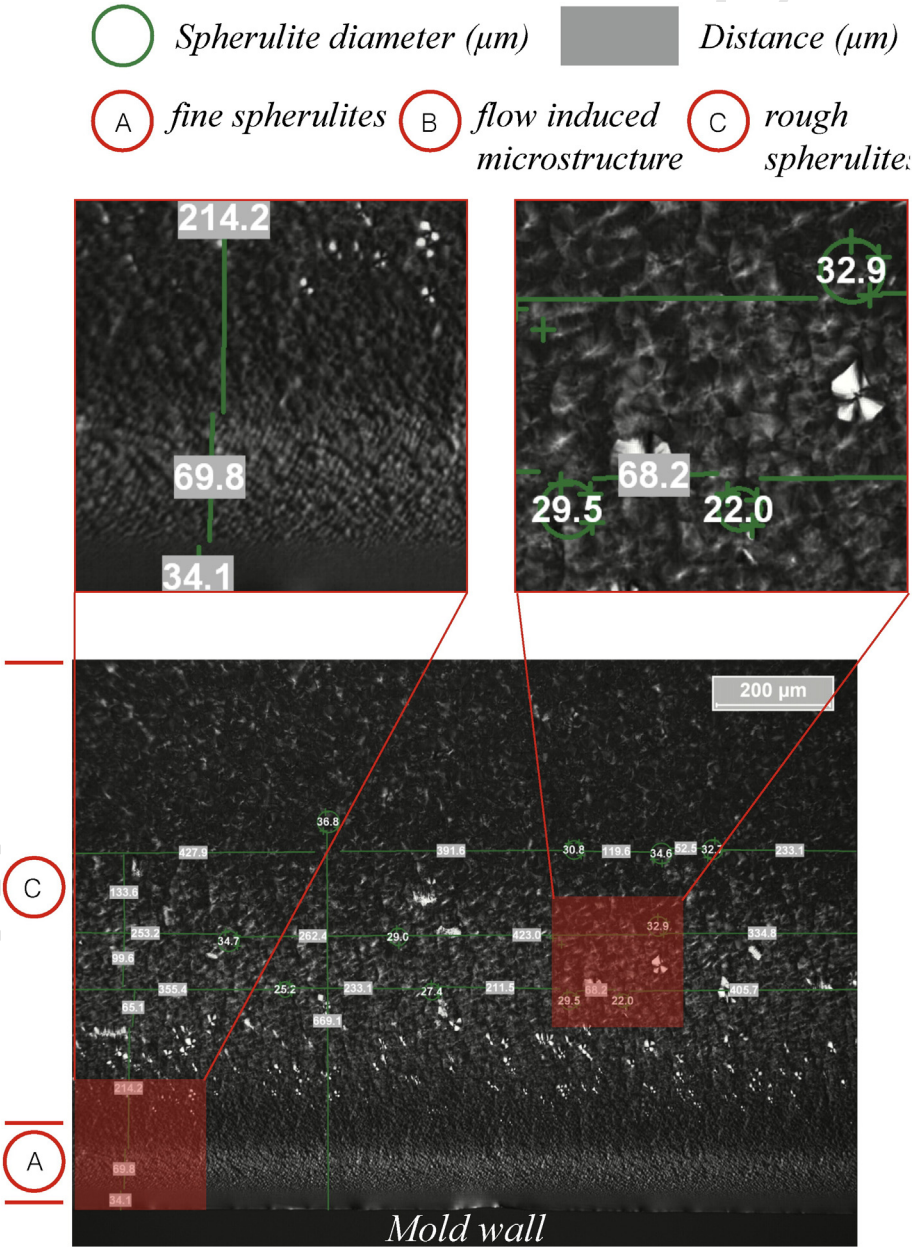

Fig. 17. Sections at *S1* location — lengthwise.

Please cite this article as: R. Spina, et al., Multiphysics simulation of thermoplastic polymer crystallization, Materials and Design (2015), http://dx.doi.org/10.1016/j.matdes.2016.01.123

in the observed domain are divided into groups every 10 μm and the size distributions are finally computed.

As a result, the entire area of interest is mapped and the spherulite distribution is obtained, as Fig. 10 shows for all points of the statistical plan.

The results illustrate that the distribution is more compact for lower values of the mold temperature, with lower values of the standard deviation. This outcome is also confirmed by the statistical analysis where each factor is evaluated in terms of t-ratio of the Lenth's method (Fig. 11). This method is considered one of the most popular techniques used to analyze unreplicated 2^p factorial experiments, as reported by Lenth [32]. The effect of the mold temperature is the highest one and its value is one order of magnitude greater than the other terms.

The same analysis was performed to measure the spherulites at the skin. Fig. 12 shows the simulated microstructures for different values of the process parameters.

Also in this case, the mold temperature is the most important factor. However, a low mold temperature causes the development of a very fine spherulite size at the mold wall because of a high temperature gradient. This condition is limited in case of a high mold temperature and the developed micro-structure is more uniform between the mold wall and core. This result is also supported by analyzing the spherulite distributions (Fig. 13).

The areal distribution of 5 μm class is the most populated for the mold temperature equal to 40 °C. An increase of the mold temperature causes an increase of the spherulite diameters up to 65 μm class whereas the injection time and temperature have a limited influence on the spherulite size, which can be seen in Fig. 14.

The simulation results were also confirmed from the experimental investigations. The manufactured part, shown in Fig. 15, was realized with the injection molding parameters represented by the triplet (2.1/220/20). The sections of interest were located along the center line, near the gate (*S1*) and in the middle of the part (*S2*). These two locations were selected to evaluate the effects of the thermal and flow-induced crystallization on final microstructure.

Microtome samples were cut from the bulk sections and inspected using a polarized optical microscope to analyze the appearance of different microstructures and their thickness. The lengthwise section at the *S1* position, shown in Fig. 16, presents a multilayer structure with at least three distinct morphologies. The formation of these layers is directly induced by highly inhomogeneous conditions due to temperature gradients and shear applied during filling.

The first layer, denoted with *A*, positioned near the mold wall, has a thickness of 140 to 150 μm. This thin layer is characterized by an amorphous structure with very fine dispersed spherulites with a size close to the resolution of the optical microscopy. This microstructure is caused by the rapid cooling experienced during processing that promotes high nucleation coupled to a low crystal growth. The second layer, denoted with *B*, is directly influenced by the polymer flow. The microstructure is highly oriented along the flow and a sharp transition with the skin exits. The microstructure is characterized by non-uniform morphologies oriented in the flow direction such as fibrous crystalline structures (shish-kebabs) and small spherulites. The extension of this layer is approximately 380 μm. The last layer, denoted with *C*, consists of an unoriented coarse spherulite structure. Each spherulite presents a central dark cross (Maltese cross) with wings coincident with the respective planes of polarizer and analyzer. The resulting structure reveals a disorientation (relaxation) of the melt in this layer before crystallization has started, followed by a fully developed crystallization growth in the quiescent melt (Varja, [33]). The average size of spherulites is about 37 μm, taking into account the non-equatorial cross sections and the effect of the microtoming cutting.

The lengthwise section at the *S2* position, shown in Fig. 17, presents a multilayer structure with at least two distinct morphologies. In this case, the cooling effect is predominant in respect to the flow effects. The first layer, denoted with *A*, is very similar to that previously investigated. The main difference is that the thickness is reduced to 100 μm. The second layer, denoted with *C*, consists of coarse spherulites with an average size of 38 μm.

The variations of the mold and melt temperatures were also investigated (Fig. 18). It is possible to note that section with the lower mold temperature (2.1/240/40) presents a spherulite size that increases from the mold wall to part core, with a very fine microstructure at the mold wall. On the contrary, the section with a high mold temperature (2.1/280/80) presents a uniform spherulite size along the entire section.

These results confirm again the efficiency of the computational models in predicting the final microstructure of the injection molding parts.

7. Conclusions

The multiscale simulations of the polymer crystallization have been successfully implemented. The numerical results of the spherulite evolution and final microstructures are in good agreement with the experimental tests, confirming the robust design of proposed framework.

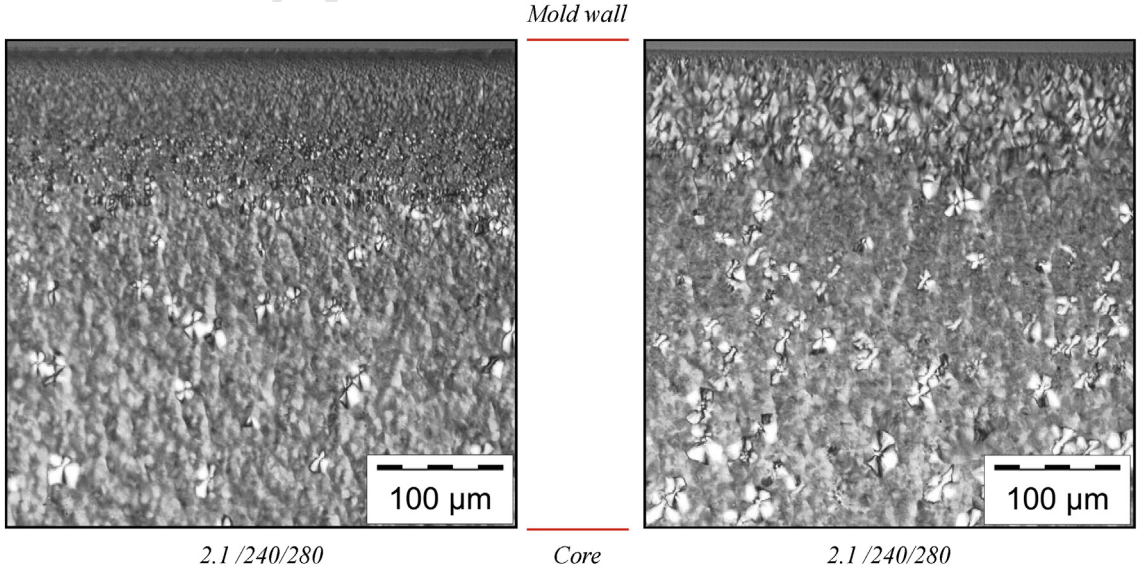

Fig. 18. Section with (2.1/240/40) and (2.1/280/80).

The research shows that the framework is able to reproduce the crystallization kinetics under non-isothermal and temperature-gradient conditions, on a macro- and micro-scale. This scheme provides an effective description for the macro/μ behavior of non-isothermal flow particles and related developed microstructures by exactly computing the melt motions while considering the inner properties. The results pointed out that different processing condition, producing the same crystallization degree, led to an important variation in spherulite sizes and distributions. For this reason, the processing conditions need to be carefully analyzed based on the additional consideration of morphology to achieve desired mechanical properties for a plastic part.

Further research should be addressed to develop a robust homogenization scheme allowing the re-computation of the thermal and flow properties. In addition, several theoretical issues associated to the sensitivity of the material properties should be the focus of future studies.

Acknowledgment

The authors wish to thank Prof. Luigi Tricarico of DMMM (Politecnico di Bari) and Nikolai Borchmann of IKV (RWTH Aachen) for their precious support during the research activities.

The authors acknowledge funding for this work from Deutscher Akademischer Austauschdienst (DAAD), Deutsche Forschungsgemeinschaft (DFG) as part of the Cluster of Excellence "*Integrative Production Technology for High-wage Countries*" and the Italian National Operative Program as SMATI project (PON01_02584).

References

[1] Z. Lv, Y. Yang, R. Wu, Y. Tong, Design and properties of a novel nucleating agent for isotactic polypropylene, Mater. Des. 37 (2012) 73–78.
[2] T. Xu, J. Yu, Z. Jin, Effects of crystalline morphology on the impact behavior of polypropylene, Mater. Des. 22 (2001) 27–31.
[3] Y. An, L. Gu, Y. Wang, Y.-M. Li, W. Yang, B.-H. Xie, M.-B. Yang, Morphologies of injection molded isotactic polypropylene/ultra high molecular weight polyethylene blends, Mater. Des. 35 (2012) 633–639.
[4] N.K. Madi, Thermal and mechanical properties of injection molded recycled high density polyethylene blends with virgin isotactic polypropylene, Mater. Des. 46 (2013) 35–441.
[5] Q. Zeng, L. Zhang, Y. Xu, L. Cheng, X. Yan, A unified view of materials design: two-element principle, Mater. Des. 30 (2009) 487–493.
[6] H.E.H. Meijer, L.E. Govaert, Mechanical performance of polymer systems: the relation between structure and properties, Prog. Polym. Sci. 30 (2005) 915–938.
[7] S.-C. Dai, F. Qi, R.I. Tanner, Strain and strain-rate formulation for flow-induced crystallization, Polym. Eng. Sci. 46 (2006) 659–669.
[8] E. Koscher, R. Fulchiron, Influence of shear on polypropylene crystallization: morphology development and kinetics, Polym. J. 43 (2012) 6931–6942.
[9] E. Ratajski, H. Janeschitz-Kriegl, Flow-induced crystallization in polymer melts: on the correlation between nucleation and specific work, Polym. Bull. 68 (2012) 1723–1730.
[10] J. Guo, K.A. Narh, Simplified model of stress-induced crystallization kinetics of polymers, Adv. Polym. Technol. 21 (2002) 214–222.
[11] Y.-G. Zhou, C.-Y. Shen, C.-T. Liu, Q. Li, L.-S. Turng, Computational modeling and numerical simulation of flow-induced crystallization kinetics during injection molding of polyethylene terephthalate, J. Reinf. Plast. Compos. 29 (2010) 76–85.
[12] K.H. Kim, A.I. Isayev, K. Kwon, Flow-induced crystallization in the injection molding of polymers: A thermodynamic approach, J. Appl. Polym. Sci. 95 (2005) 502–523.
[13] M. Zinet, R.E. Otmani, M. Boutaous, P. Chantrenne, Numerical modeling of nonisothermal polymer crystallization kinetics: flow and thermal effects, Polym. Eng. Sci. 50 (2010) 2044–2059.
[14] R. Zheng, P.K. Kennedy, A model for the post-flow induced crystallization: General equations and predictions, J. Rheol. 48 (2004) 823–842.
[15] R. Zheng, R.I. Tanner, et al., Modeling of flow-induced crystallization of colored polypropylene in injection molding, Korea-Australia Rheol. J. 22 (2010) 151–162.
[16] L. Shangguan, Y. Yang, J. Yang, Double scale coupling model of plastic injection molding, Adv. Mater. Res. 472-475 (2012) 2148–2151.
[17] Y. Rong, H.P. He, W. Cao, C.Y. Shen, J.B. Chen, Multi-scale molding and numerical simulation of the flow-induced crystallization of polymer, Comput. Mater. Sci. 67 (2013) 35–39.
[18] C. Ruan, K. Liang, L. Guo, W. Li, Computer modeling and simulation for 3D crystallization of polymers. I. Isothermal case, Polym. Plast. Technol. Eng. 51 (2012) 810–815.
[19] S. Wienke, M. Spekowius, A. Dammer, D. an Mey, C. Hopmann, M.S. Müller, Towards an accurate simulation of the crystallisation process in injection moulded plastic components by hybrid parallelisation, Int. J. High Perform. Comput. Appl. 28 (2014) 356–367.
[20] S. Osher, J.A. Sethian, Fronts propagating with curvature-dependent speed: algorithms based on Hamilton–Jacobi formulations, J. Comput. Phys. 79 (1998) 12–49.
[21] E. Olsson, G. Kreiss, A conservative level set method for two phase flow I, J. Comput. Phys. 210 (2005) 225–246.
[22] E. Olsson, G. Kreiss, S. Zahedi, A conservative level set method for two phase flow II, J. Comput. Phys. 225 (2007) 785–807.
[23] R. Spina, M. Spekowius, C. Hopmann, Multi-scale thermal simulation of polymer crystallization, Int. J. Mater. Form. (2014)http://dx.doi.org/10.1007/s12289-014-1169-8.
[24] J.I. Lauritzen, J.D. Hoffman, Theory of formation of polymer crystals with folded chains in dilute solution, J. Res. Natl. Bur. Stand. 64A (1960) 73–102.
[25] J.D. Hoffman, G.T. Davis, J.I. Lauritzen, The Rate of Crystallization of Linear Polymers with Chain Folding, Treatise in Solid State Chemistry, Plenum Press, 1976 3.
[26] S. Mueller, E.W. Llewellin, H.M. Mader, The rheology of suspensions of solid particles, The rheology of suspensions of solid particles, Proc. R. Soc. London, Ser. A 466 (2010) 1201–1228.
[27] M.L. Williams, R.F. Landel, J.D. Ferry, The temperature dependence of relaxation mechanisms in amorphous polymers and other glass-forming liquids, J. Am. Chem. Soc. 77 (1955) 3701–3707.
[28] R. Spina, M. Spekowius, R. Dahlmann, C. Hopmann, Analysis of polymer crystallization and residual stresses in injection molded parts, Int. J. Precis. Eng. Manuf. 15 (2014) 89–96.
[29] M. Spekowius, R. Spina, C. Hopmann, Mesoscale simulation of the solidification process in injection moulded parts, J. Polym. Eng. (2015)http://dx.doi.org/10.1515/polyeng-2014-0223 (in press).
[30] W.P. Cox, E.H. Merz, Correlation of dynamic and steady flow viscosities, J. Polym. Sci. 28 (1958) 619–622.
[31] H. Zuidema, G.W.M. Peters, H.E.H. Meijer, Influence of cooling rate on pVT-data of semicrystalline polymers, J. Appl. Polym. Sci. 82 (2001) 1170–1186.
[32] R.V. Lenth, Quick and easy analysis of unreplicated factorials, Technometrics 31 (1989) 469–473.
[33] J. Varja, Supermolecular structure of isotactic polypropylene, J. Mater. Sci. 27 (1992) 2557–2579.

Please cite this article as: R. Spina, et al., Multiphysics simulation of thermoplastic polymer crystallization, Materials and Design (2015), http://dx.doi.org/10.1016/j.matdes.2016.01.123